FISEVIER

Contents lists available at ScienceDirect

## BBA - Gene Regulatory Mechanisms

journal homepage: www.elsevier.com/locate/bbagrm





# Identifying distinct heterochromatin regions using combinatorial epigenetic probes in live cells

Agnes Mendonca <sup>a, 1</sup>, Oscar F. Sánchez <sup>a, 1</sup>, Junkai Xie <sup>a</sup>, Ana Carneiro <sup>a</sup>, Li Lin <sup>a</sup>, Chongli Yuan <sup>a, b, \*</sup>

- <sup>a</sup> Davidson School of Chemical Engineering, Purdue University, West Lafayette, IN 47906, USA
- <sup>b</sup> Purdue University Center for Cancer Research, Purdue University, West Lafayette, IN 47906, USA

#### ARTICLE INFO

Keywords: Heterochromatin DNA methylation Histone methylation

## ABSTRACT

The 3D spatial organization of the genome controls gene expression and cell functionality. Heterochromatin (HC), which is the densely compacted and largely silenced part of the chromatin, is the driver for the formation and maintenance of nuclear organization in the mammalian nucleus. It is functionally divided into highly compact constitutive heterochromatin (cHC) and transcriptionally poised facultative heterochromatin (fHC). Long regarded as a static structure, the highly dynamic nature of the heterochromatin is being slowly understood and studied. These changes in HC occur on various temporal scales during the cell cycle and differentiation processes. Most methods that capture information about the heterochromatin are static techniques that cannot provide a readout of how the HC organization evolves with time. The delineation of specific areas such as fHC are also rendered difficult due to its diffusive nature and lack of specific features. Another degree of complexity in characterizing changes in heterochromatin occurs due to the heterogeneity in the HC organization of individual cells, necessitating single cell studies. Overall, there is a need for live cell compatible tools that can stably track the heterochromatin as it undergoes re-organization. In this work, we present an approach to track cHC and fHC based on the epigenetic hallmarks associated with them. Unlike conventional immunostaining approaches, we use small recombinant protein probes that allow us to dynamically monitor the HC by binding to modifications specific to the cHC and fHC, such as H3K9me3, DNA methylation and H3K27me3. We demonstrate the use of the probes to follow the changes in HC induced by drug perturbations at the single cell level. We also use the probe sets combinatorically to simultaneously track chromatin regions enriched in two selected epigenetic modifications using a FRET based approach that enabled us tracking distinctive chromatin features in situ.

#### 1. Introduction

The mammalian nucleus is functionally divided into several regions comprising primarily of the chromatin, the nucleolus, and transcription factories [1]. Gene rich regions tend to be loosely compacted (euchromatin or EC) and are commonly found near the center of the nucleus. Densely compacted, largely gene poor regions [2–3] (heterochromatin or HC) are most abundant near the nuclear periphery [4]. Accumulating evidence suggests that the 3D spatial arrangement of chromatin largely encodes cell functionality [5–6], dictates inter- and intra- chromosomal interactions [7], partially programs transcription profile [8], and thus ultimately determines the phenotype [9]. In healthy cells, euchromatin and heterochromatin regions typically have well-defined boundaries

which are essential for distinctive gene activity and maintaining integrity during cellular processes [10].

Heterochromatin formation is the driving force behind the observed 3D architecture of the genome and forms a basis for understanding the spatial organization within the nucleus. The formation of heterochromatin occurs very early in development and is crucial for differentiation [11], as well as the establishment and maintenance of nuclear organization in mammalian cells [12–13]. Repetitive DNA regions and developmentally regulated genes are the major components of HC within the genome [2]. Functionally, heterochromatin may be divided into two sub-classes [2,14]: *i.* constitutive heterochromatin (cHC) which is highly stable, heavily compacted, and gene poor, and, *ii.* facultative heterochromatin (fHC) which tends to be less compacted, developmentally

<sup>\*</sup> Corresponding author at: Davidson School of Chemical Engineering, 480 Stadium Mall Drive, Purdue University, West Lafayette, IN 47906, USA. *E-mail address:* cyuan@purdue.edu (C. Yuan).

<sup>&</sup>lt;sup>1</sup> These authors contributed equally to the work.

regulated, and transcriptionally poised. The functional distinction between cHC and fHC is important because though both are transcriptionally silent, fHC retains the potential to interconvert between cHC and EC [15].

Both the cHC and fHC modulate chromatin to maintain nuclear stability and prevent the access of transcriptional machinery to repetitive DNA elements, curtailing their transcription and recombination. The boundaries and spatial organization of both the cHC and fHC must be maintained. Disruptions in the cHC and fHC can result in genomic instability [16-17], transcription of transposable elements and silenced repeats [18], and loss of genomic organization. For instance, heterochromatin de-condensation is commonly seen in cancer cells, such as in breast and ovarian cancer where the inactive X chromosome is decompacted leading to the expression of X linked genes [19]. The dramatic loss of heterochromatin at the nuclear periphery, leading to poor staining in malignant cancer cells, has long been used as a maker by pathologists to identify specific cancers [20]. The destabilization of HC and subsequent epigenomic instability is, however, an understudied topic area in cancer biology warranting careful studies. The distinction between cHC and fHC is difficult to accomplish by conventional cytological stains [14]. Delineating these two areas is thus of key importance in processes where the heterochromatin is disrupted.

HC is typically identified in single cells via the simple stains that bind to DNA. These include 4'6-diamidino-2-phenylindole (DAPI) for fixed cells and Hoechst 33342 for live cells, which primarily bind to AT-rich heterochromatin regions, thus differentiating it from the euchromatin regions of lower DNA density. Other approaches to identify heterochromatin are banding and FISH [21–22], which rely on the tightly compacted nature of heterochromatin DNA, or the use of specific DNA sequences, respectively, to identify heterochromatin regions. The distinction between fHC and cHC, however, has been difficult to accomplish without the use of antibodies specific to epigenetic marks found at these regions [23]. For instance, the cHC is primarily characterized by a high density of H3K9me3 and DNA methylation [2] while the fHC is enriched in H3K27me3 [14]. However, antibody-based methods require a fixation step which is not conducive to live cell applications.

In this work, we present an approach to monitor fHC and cHC regions based on epigenetic readouts. The probes directly inform the spatial distribution and abundance of epigenetic modifications and thus offer a convenient tool to reveal the contributions of HC to various biological processes.

## 2. Materials and methods

## 2.1. Construction and verification of the heterochromatin probes

To identify and quantify epigenetic modifications (H3K9me3, H3K27me3 and DNA methylation (5mC)), we have engineered protein probes based on a tandem repeat strategy as we detailed in our previous work [24-25] and literature [26-28]. This tandem repeat strategy, in which adjacent repeats of the same epigenetic "reader" domain are linked via a flexible linker to form multimeric constructs (e.g. dimer, trimer, etc.), was adopted due to the enhancement in the epigenetic target recognition and affinity. Native epigenetic domains, specifically chromo-domain of chromodomain Y protein (CDY), chromodomain of the Polycomb 2 domain (PC2), and the methyl-binding domain (MBD) of the MBD1 protein were selected for detecting H3K9me3, H3K27me3, and 5mC, respectively. These domains were selected based on their high affinity to epigenetic marks as well as high selectivity [27,29-31]. Among the different constructs that can be obtained via tandem repeats (e.g., monomer, dimer, and tetramer), the dimeric construct was found optimal in identifying the epigenetic modification of interest while larger number of repeat units (e.g., four repeats) did not further improve the resolution of our probes and may create steric hindrance for targetbinding as we shown in our previous work [24]. Each probe thus contains a nuclear localization sequence followed by a glycine-serine (GS) flexible linker and two (di-) repeats of reader domains fused to a fluorescent protein (i.e., mEGFP and mCherry) via a GS flexible linker (Fig. 1A). The probes were cloned into a mammalian expression vector, pRK5, (Addgene (plasmid number: 18696), Cambridge, MA) and transiently transfected into the cells. The amino acid sequences of all probes containing dimeric recognition domains are shown in Table S1 (Supporting Information).

Taken H3K27me3 as an example, we validated the in vitro and in situ performance of our designed probes following our published protocols [24–25]. Briefly, we determined the binding affinity of H3K27me3 probes to histone peptides with sequences detailed in Fig. S1A (Supporting Information) via Bio-Layer Interferometry (BLI). BLI results suggest that the H3K27me3 probe exhibits a significant preference for H3K27me3 peptides as shown in Fig. S1B (Supporting Information)). The  $K_D$  value of the dimeric PC2 protein sensor to H3K27me3 was determined to be  $0.42 \pm 0.15 \ \mu M$  (Fig. S1C (Supporting Information)), which is lower than the 5  $\mu M$  reported for PC2 [32].

*In situ* validation of the H3K27me3 probe was accomplished via a colocalization assessment between the probe and a validated anti-H3K27me3 antibody (ab192985, Abcam). The fluorescence pattern of H3K27me3 probes and antibody was analyzed via a correlation analysis, i.e., Mander's Colocalization Analysis and was found to be in a close correlation (Mander's coefficients' > 0.95).

To ensure that our fluorescent signal arises specifically from the binding of heterochromatin recognition domain, we introduced mutations to the selected H3K9me3 (W28V) and H3K27me3 (Y19A) recognition domain. These mutations were located at the conserved aromatic cage known for recognizing H3K9me3 [33] and H3K27me3 [34–35], respectively. Typical images of cells transfected with the wild-type and mutated H3K9me3 and H3K27me3 probes were summarized in Fig. S2A and B (Supporting Information), respectively. The probes with the mutated recognition domain exhibited a diffusive fluorescent pattern inside nucleus lacking any foci-like features. Furthermore, the calculated volumetric fraction of mutant probes is lower than 1% (Fig. S2C (Supporting Information)). The captured signal by the mutant probes represents less than 0.02 of the relative epigenetic targets compared to the wild-type (Fig. S2D, (Supporting Information)) suggesting that there is no binding between the mutant probe and the epigenetic target.

## 2.2. Mammalian cell culture and transfection

Human embryonic kidney 293T (HEK293T) cells were maintained following standard cell culture protocols [36]. Live cell tracking were accomplished using 8 well µ-slides or grid slides (ibidi, Fitchburg, WI) as we descried previously [31]. HEK293T cells were exposed to various epigenetic drugs to perturb the intrinsic epigenetic modification levels. Generally, for all drug exposure experiments, cells were exposed to the drug when they attained a confluence of 50-60%. Concentrations of drugs were selected to effectively alter the levels of the epigenetic targets while minimally affecting cytotoxicity [37-42]. Specifically, Bix-01294, a histone methyltransferase inhibitor, has an IC50 of 1.9  $\mu M$ and 0.7  $\mu M$  for G9a and GLP HMTases, respectively [43–44], and was used to lower the H3K9me3 levels at 3 and 5  $\mu$ M. RG108, a DNMT1 inhibitor, was used to lower the DNA methylation level at CpG dinucleotides [45-46]. RG108 was reported to have an IC50 of 115 nM [45] to 390  $\mu$ M [47] and low cytotoxicity [45,47]. RG108 was used at a concentration of 50 and 100  $\mu M$  in this study. DZNep can affect various histone methyltransferases [48] with low cytotoxicity [49], and was thus used to reduce the levels of H3K27me3 at 3 and 5  $\mu M$ . Fig. S3 (Supporting Information) shows that the selected drug concentrations do not significantly altering the growth of HEK293T cells (p = 0.05).

## 2.3. Analysis of epigenetic modification levels

Global changes in epigenetic modifications were analyzed via

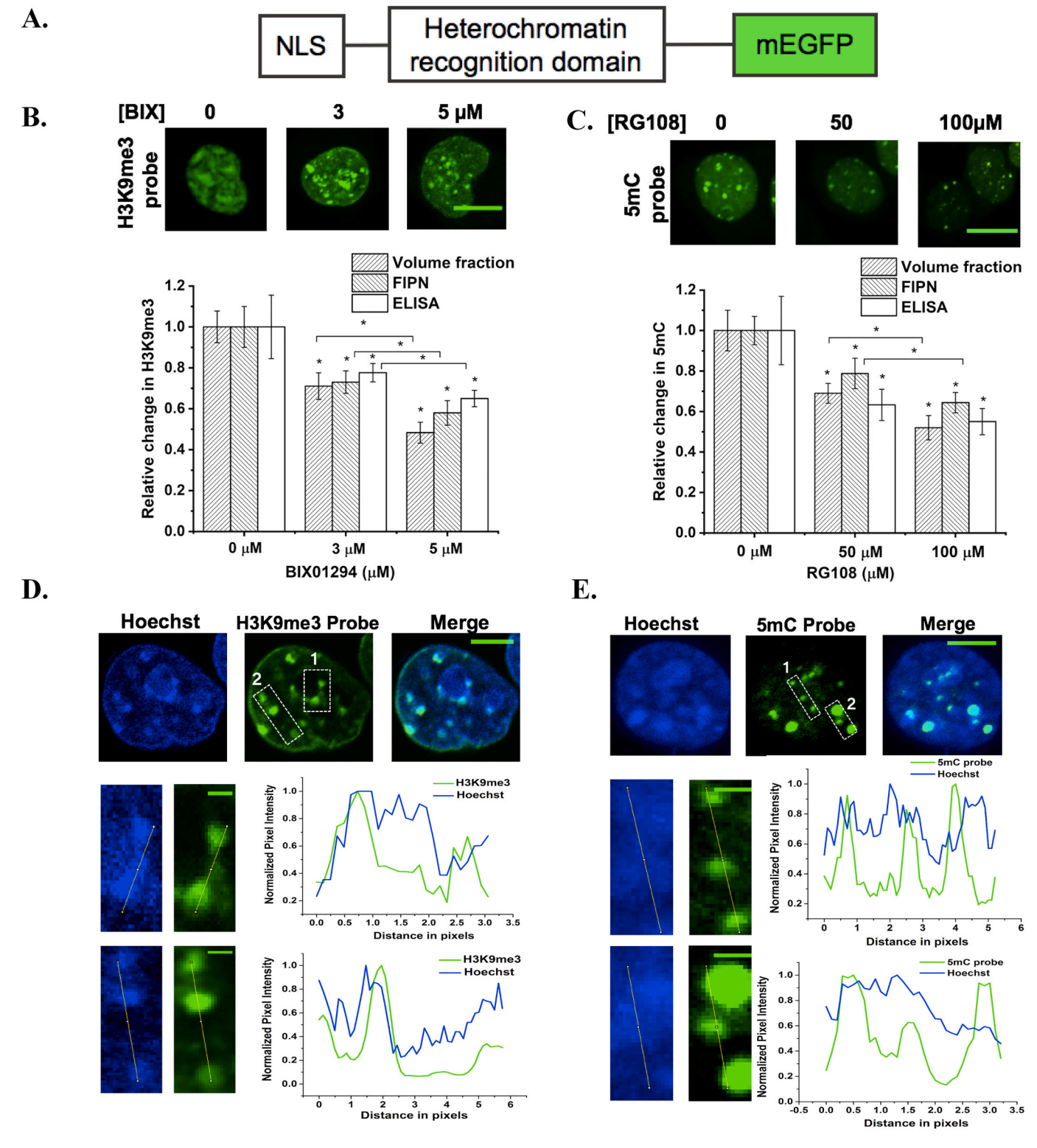


Fig. 1. A. Schematic of the heterochromatin recognition probes. B. Top panel: Maximum intensity projections of the 3D confocal stacks of the cells expressing the H3K9me3 probes and treated with increasing concentrations of BIX01294. Bottom panel: Corresponding decrease in relative H3K9me3 levels upon drug treatment as captured by ELISA and volumetric analysis. C. Top panel: Maximum intensity projections of the 3D confocal stacks of the cells expressing the 5mC probes and treated with increasing concentrations of RG108. Bottom panel: Corresponding decrease in relative 5mC levels upon drug treatment. Scale bar =  $10 \mu m$ . \*: p < 0.05, n = 100 for volumetric/intensity analysis, and 3 for ELISA. Data = mean  $\pm$  S.D. D and E. Co-stained images of cells expressing the H3K9me3 or 5mC probe with a DNA dye (Hoechst). Significant heterochromatin regions are highlighted in regions 1 and 2 of both cells to demonstrate the improved spatial resolution offered by both probes. Scale bar =  $10 \mu m$  in top panel and  $2 \mu m$  in zoomed in regions of the bottom panel.

commercial ELISA kits (Total H3 ELISA (cat #53110, Active Motif, CA), H3K9me3 ELISA (cat #53109, Active Motif, Carlsbad, CA), H3K27me3 ELISA (cat #53104, Active Motif, CA) and Global DNA methylation ELISA (cat #,55017, Active Motif, Carlsbad, CA)). Relative changes in epigenetic modification levels were determined by comparing the modification level of our drug treated sample to an untreated control.

#### 2.4. Immuno-fluorescence staining

Transfected cells were co-stained with commercial antibodies. Specifically, cells transfected with the probes were fixed using methanol or 4% paraformaldehyde as a fixative agent [50]. After a one-hour block with 1% BSA in PBS, cells were incubated with the respective primary antibody for 1 h at RT: rabbit Anti-Histone H3K9me3 antibody (ab8898, Abcam, Cambridge, MA), rabbit Anti-Histone H3K27me3 antibody (39157, ab192985, Abcam, Cambridge, MA) and mouse Anti 5-methylcytosine antibody (61480, Active Motif, Carlsbad, CA). For the latter (5mC-antibody), an additional denaturing step was required between blocking and incubation with 5mC antibody since the 5mC-antibody binds only to single-stranded DNA. The denaturing step was carried out using HCl 2N and incubating for 30 min at RT followed by three PBS washes. Cells were then incubated for 1 h at RT with the secondary antibody: Goat-anti rabbit Alexa Fluor 568 (Abcam, Cambridge, MA) or Donkey-anti-mouse Alexa Fluor 647 (Millipore, Billerica, MA). Coverslips were washed three times with PBS and mounted using glycerol on slides for imaging. DNA staining was performed using Hoechst stain (Sigma, St Louis, MO) at a 1:500 dilution for 10 min.

#### 2.5. Image acquisition and analysis

Live or fixed cells were imaged on a Nikon Eclipse Ti-E microscope equipped with a  $60\times$  oil immersion objective lens. 20–30 X-Y optical sections were imaged to collect Z-stack images. GFP and mCherry were excited using a 488 nm and 534 nm laser excitation source, respectively. For experiments involving colocalization of different probes, two laser lines were used in a sequential mode to avoid bleed-through effects. The confocal pinhole was set to S (small) and low laser intensities were used to avoid photo-bleaching effects.

Images for sensitized FRET measurements were acquired in a sequential manner in the GFP, mCherry and FRET channels at RT. The filter sets employed were Donor/GFP (Excitation: 488/2 nm, Emission: FITC), Acceptor/mCherry (Excitation: 532/2 nm, Emission: Cy5) and FRET (Excitation: 488/2 nm, Emission: Cy5). To determine the spectral bleed-through of GFP into the FRET channel, a donor-only sample was imaged using Donor/GFP and FRET settings. Direct excitation of the acceptor was calculated by imaging an acceptor-only sample in the Acceptor/mCherry and FRET channels. Donor- and acceptor-emission of each sample was also determined and used as a factor to normalize FRET signal and thus correcting for variations in protein expression levels across cells.

Z-stack images were used to perform volumetric intensity fraction analysis. Specifically, we first determined background signal using cytoplasmic fluorescence intensity. Fluorescence signal over background in each 2D slice was determined by subtracting the background. These signals were subsequently integrated to get the 3D voxels via the Voxel Volume plugin of ImageJ after threshold segmentation. Colocalization analysis was performed using the ImageJ plugin JACOP. Thresholding was performed using Costes method [51] to calculate the Mander's coefficients. FRET analysis was performed using the ImageJ plugin PixFRET [52]. All other images were analyzed via CellProfiler [53] using a customized pipeline (Supporting Information, MethodsX).

## 2.6. Statistics

All statistical analysis and error propagation calculations were performed using Graphpad Prism by a one-way ANOVA analysis followed by post-hoc Tukey's test, considering p<0.05 to be statistically significant. OriginPro and Graphpad Prism were both used for creating figures and graphs. A minimum of 100 cells was analyzed for calculating the colocalization coefficients and volume fractions. ELISA was performed on a minimum of three biological independent samples with >2 technical repeats of each. FRET analysis was performed for n>30 cells.

#### 3. Results and discussion

## 3.1. Quantifying constitutive heterochromatin (cHC) levels

A microscopy-based approach can be instrumental in examining the spatial distribution of heterochromatin associated modifications within the cell. We tested the H3K9me3 and 5mC probes in HEK293T cells (live cell images in Fig. S4 (Supporting Information), probe schematic in Fig. 1A) and observed the characteristic cHC distribution. The H3K9me3 probe is localized at the nuclear periphery [54] and around the perinucleolar regions forming distinct ring-like structures around the nucleolus [55–57]. The 5mC probe shows a pattern of small punctate dots, corresponding to dense regions of DNA methylation [27,58].

Quantification of cHC was performed by perturbing the system by the addition of epigenetic drugs and measuring the changes in cHC levels using the H3K9me3 and 5mC probes. BIX-01294 (Sigma, St. Louis, MO) a histone methyltransferase (G9a and GLP HMTase) inhibitor [43–44] was used to lower the H3K9me3 levels. The drug concentrations chosen for BIX-01294 treatment were 3 and 5  $\mu$ M respectively in order to minimize toxicity effects and morphological changes in cells [43]. At the specified [BIX01294], there is a significant drop in the H3K9me3 levels measured by the total volume occupied by the probe in the nucleus and the mean foci intensity per nuclei (volume fraction and FIPN respectively in Fig. 1B) which closely matches the values obtained using a commercial ELISA kit. Visualizing the changes induced by BIX01294, in Fig. 1B, top panel, fewer foci of H3K9me3 and lesser modification levels at the nuclear periphery are visible. As shown in Fig. 1B, the drop in the volume fraction occupied by bound probes is ~28% and 52% of the original value at [BIX01294] = 3 and 5  $\mu M$ . A similar reduction in H3K9me3 levels is observed via FIPN analysis, ~26 and 41% for BIX01294 of 3 and 5  $\mu$ M, respectively. The drop in modification levels is significantly different with p < 0.05 as compared to the control sample. The H3K9me3 probe is also able to resolve the differences in H3K9me3 levels at two different drug concentrations. We further challenged our H3K9me3 probes with chaetocin, a nonspecific inhibitor for histone methyl transferase (SUV39H1) that has an IC<sub>50</sub> of  $0.11-0.8 \mu M$  [59–60]. Chaetocin treatment results in a reduction of ~31 and 48% of H3K9me3 at 0.1 and 0.2 µM, respectively, quantified via FIPN (Fig. S5 (Supporting Information)).

Similarly, the volume fraction occupied by the 5mC probe drops significantly as the methylation levels are lowered by the DNMT inhibitor RG108 (see Fig. 1C). As the number and intensity of the foci decrease, the volume fraction drops to  $\sim\!\!30$  and 48% of the original value, agreeing with the observed FIPN reductions of  $\sim\!\!22$  and 38% (statistically significant with a p<0.05) at [RG108] of 50 and 100  $\mu\text{M}$ , respectively. These numbers agree with the ELISA values quantifying the relative DNA methylation levels.

To assess the spatial resolution offered by the probes, we compared the binding pattern with commonly used live cell dyes for staining cHC. The Hoechst dye is a non-specific DNA binding agent that is routinely used to stain nuclei and heterochromatin in live and fixed cells [61]. In Fig. 1D (top panel), cells expressing the H3K9me3 probe were counterstained with Hoechst to compare the features delineated by both methods. The overlap between the H3K9me3 probe signal and the Hoechst dye are presented in the merge channel and show a good overlap. However, upon zooming into certain regions of interest, the probe offers higher spatial resolution as compared to the non-specific DNA stain. A pixel plot analysis of typical cHC regions at the perinucleolus and the nuclear periphery (see Regions 1 and 2, Fig. 1D),

show that a diffusive signal in obtained by the Hoechst dye and sharply defined peaks are obtained in the H3K9me3 probe channel. The specificity of the probe for H3K9me3 leads to a higher signal-to-noise ratio as compared to the diffuse and poorly resolved signal obtained in the Hoechst channel. The results obtained with our 5mC probe closely mirror the H3K9me3 probe. There is a significant overlap between the 5mC probe and the Hoechst signal which binds non-specifically to DNA primarily at heterochromatin locations. Since the heterochromatin is enriched in DNA, this dye even acts as an indirect measure of DNA methylation and has been used to validate MBD1 probes in previous works [27,58]. However, the resolution offered by MBD1 based 5mC probes is much greater than the Hoechst dye as can be seen in zoomed in Regions 1 and 2 of the cell in Fig. 1E, showing sharp peaks of DNA methylation islands. Moreover, since commercially available DNA methylation antibodies bind only to single stranded DNA, they require an additional HCl denaturing step for binding. The non-toxic and live cell compatible feature of the 5mC probe, coupled with its improved resolution make it an attractive alternative to assess DNA methylation

## 3.2. Quantifying facultative heterochromatin levels

The success of both the H3K9me3 and 5mC probes in capturing regions of cHC lead us to examine modifications associated commonly with the facultative heterochromatin (fHC). The fHC is also transcriptionally silent but remains poised to convert to euchromatin under temporal or spatial control (such as during development or cell-cycle stages or changes in 3D nuclear reorganization [14]). Interestingly, since the fHC occupies an intermediate state between cHC and EC, it is often indistinguishable from both by conventional staining methods. The epigenetic signatures of the fHC are however quite distinctly different from cHC and EC. The epigenetic modification H3K27me3 often in tandem with DNA methylation is enriched at various fHC locations such as the inactive X chromosome (Xi) [62], autosomally imprinted genomic loci [63], and HOX gene clusters [64].

We developed a H3K27me3 probe that could capture dynamic changes in this modification level. The PC2 domain was used as the epigenetic reader domain that binds to H3K27me3 sites [65]. Images of HEK293T cells expressing the probe are shown in Fig. 2A (top panel). The signal is more diffused as compared to the denser H3K9me3 and 5mC modifications, but the probe is successful in capturing features of H3K27me3 distribution. This includes foci of H3K27me3 and dense regions such at the inactive X chromosome which is generally present near the nuclear periphery. The pattern obtained by the H3K27me3 probe exactly matches that of commercial antibodies (see Fig. 2A, bottom panel). We quantified the extent of overlapping between the probes and the antibody in Fig. 2B, obtaining Mander's correlation coefficients, namely M1 and M2, close to 1, indicating a high degree of positive pixel-by-pixel correlation between the two channels (probe and antibody).

The quantitative ability of the probes to capture changes in H3K27me3 levels was determined using the intensity and volumetric approach described above. The drug 3-deazaneplanocin A (DZNep) which inhibits multiple histone methyltransferases was used to lower the H3K27me3 levels at a concentration of 3 and 5  $\mu$ M [49]. Images of cells exposed to the drug at various concentrations are shown in the top panel of Fig. 2C. The signal is extremely diffuse at increasing drug concentrations with most observable foci being lost (additional images are provided in Fig. S6 (Supporting Information)). The corresponding drop in H3K27me3 levels was assessed using a commercial ELISA based approach (Fig. 2C, bottom panel) showing a significant decrease in the H3K27me3 levels. The volume fractions occupied by the H3K27me3 probe drops to  ${\sim}58$  and 70% of the original value at 3 and 5  ${\mu}M$  DZNep concentrations which closely matches the relative values obtained by ELISA. FIPN analysis followed a similar trend with an H3K27me3 reduction of  ${\sim}50$  and 60% at 3 and 5  $\mu M$  of DZNep, respectively. These differences are statistically significant in both cases as compared to the

untreated control samples (p < 0.05).

The spatial resolution offered by the H3K27me3 in delineating the fHC is significantly better when compared to the Hoechst staining. At the nuclear periphery (region 1) and the perinucleolar areas (region 2) for the cell shown in Fig. 2D, the peaks obtained using the probe are sharply defined as compared to the Hoechst signal. Since the Hoechst dye does not differentiate between the cHC and fHC, the H3K27me3 probe offers an added advantage in capturing specific features of the heterochromatin.

## 3.3. Single cell dynamic trajectories of heterochromatin levels

The main goal here was to develop specific probes for the monitoring of cHC and fHC as they undergo dynamic changes at the single cell level. The H3K9me3, 5mC, and H3K27me3 probes selectively identify the cHC and fHC and may thus be used in combination to assay both regions simultaneously. We demonstrated the use of the probes in live cell tracking, by introducing an alternative fluorescent tag (mCherry) on the probes for tracking two modifications simultaneously. Drug perturbations were performed to modulate the epigenetic landscape of the chromatin. We then tracked these dynamic changes by following individual cells as they underwent normal cellular processes in the presence and absence of epigenetic drugs.

Since the cHC forms the more static part of heterochromatin, we began by monitoring dense regions of cHC identified by a high density of H3K9me3 and 5mC. The H3K9me3 and 5mC probes were simultaneously introduced into HEK293T cells to monitor changes in cHC as cells undergo growth and division. As it can be seen in Fig. 3A, at T = 0 h, the nuclei exhibit the characteristic binding pattern corresponding to H3K9me3 and 5mC distribution with a defined nuclear ring and islands of H3K9me3 and DNA methylation. The patterns overlap significantly with each other, as expected, since both probes are highly specific to cHC. The binding pattern is retained in daughter cells upon successive cell divisions. We then perturbed the system by adding a combination of drugs that affects both modification levels (BIX01294 and RG108 at 5 μM and 100 μM respectively) and monitored the variations in the cHC with time. Images obtained from dynamic tracking are presented in Fig. 3B. As early as T = 12 h post drug addition, a decline in both H3K9me3 and 5mC is seen. The intensity of binding at the nuclear periphery decreases and the number of bright foci also decreases. For the 5mC probe, we observed smaller, dimmer foci along with the accumulation of unbound probes in the nucleolus as sites of 5mC are lost. These changes are more pronounced with time, resulting in a lower fluorescent intensity per nuclei (quantified in Fig. 3E, for additional single cell images and grid slide coordinates, see Fig. S7A and S7C (Supporting Information)). The cumulative effect of adding multiple epigenetic drugs can be decoupled by studying the effects of a single drug on either H3K9me3 or 5mC levels (data for individual drug treatments presented as dashed lines in Fig. 3E, cell images in Fig. S8A and B (Supporting Information)). Firstly, the addition of RG108 appears to increase the H3K9me3 modifications in the early stages of drug exposure. This increase is maintained at T = 24 h and eventually approaches the same level as the untreated case (at T=48 h). The addition of BIX01294 modulates the H3K9me3 level as expected with steady losses seen at increasing time points. In a combinatorial effect of RG108 and BIX01294 on H3K9me3 levels, it appears that the declining effects of BIX01294 addition are offset by the increase in H3K9me3 levels induced by RG108. In examining the effect of BIX01294 on DNA methylation, a decrease in 5mC levels occurs when the cells are exposed to BIX01294. Both BIX01294 and RG108 successively lower the 5mC level with time and the cumulative effect of both drugs is slightly more pronounced than individual treatments (Fig. 3E, bottom panel). There are several possible regulatory pathways that might contribute to the crosstalk observed in these experiments. For instance, the H3K9me3 mark recruits HP1 [66] and UHRF1 [67-68], both of which have regulatory links with DNA methyltransferases. In HMT knockout MESC, a depletion of DNMT is

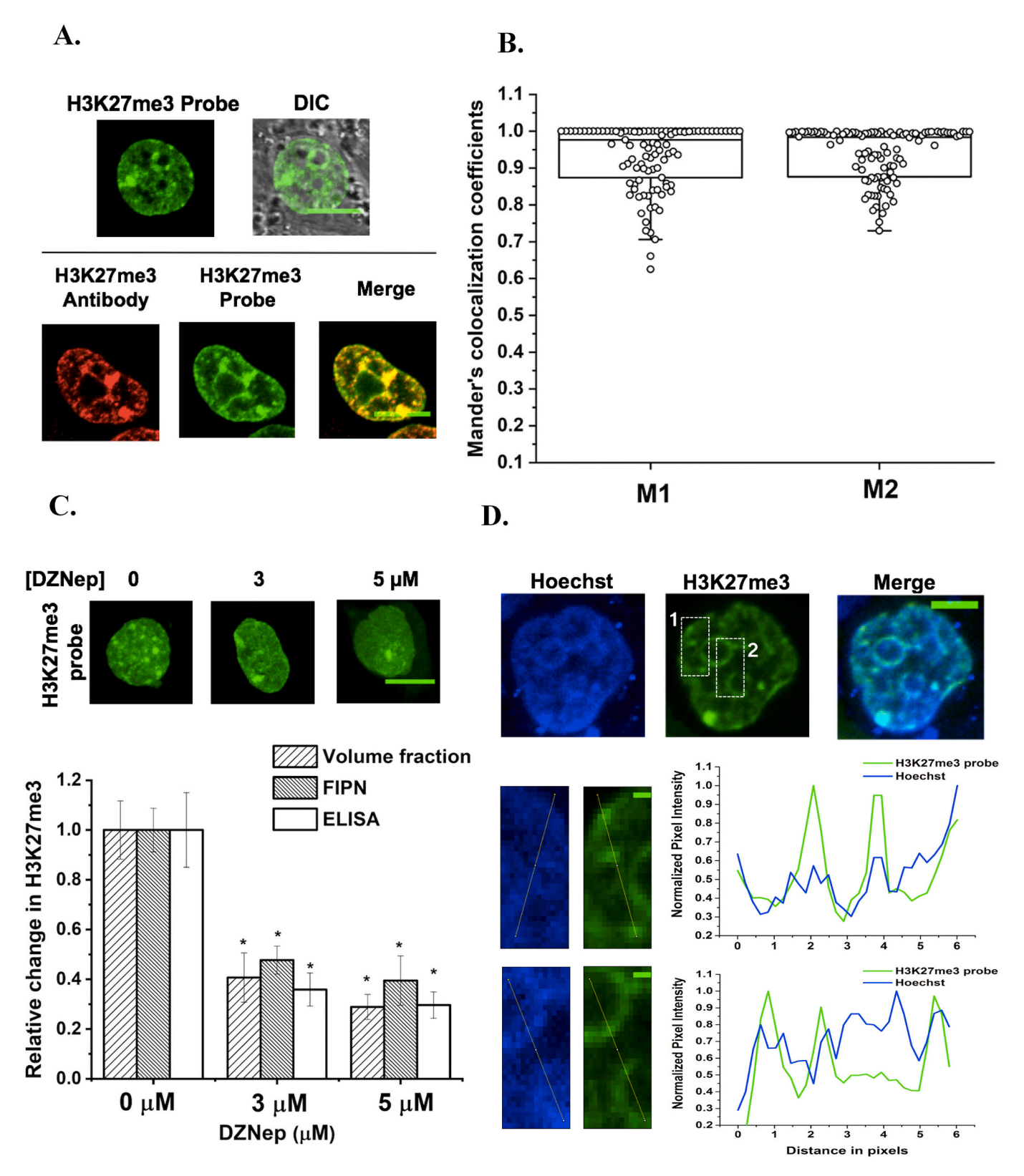


**Fig. 2. A.** Live cell images of HEK293T cells expressing the H3K27me3 probe (top panel). The cells were counterstained with a commercially obtained antibody against H3K27me3 and shows significant overlap. **B.** The Mander's correlation coefficients for the signal obtained in the probe and antibody channels. **C.** Top panel: Images of cells treated with the drug DZNep. Bottom panel: corresponding changes in H3K27me3 measured by volume fraction and ELISA. Scale bars =  $10 \, \mu m$ . \* indicates a statistically significant difference with p < 0.05, n = 100 for volumetric analysis, and 3 for ELISA. Error bars represent the standard deviation. **D.** The probe was co-stained with Hoechst dye to demonstrate the improvement in signal:noise ratio obtained by using a probe specific to the H3K27me3 modification.

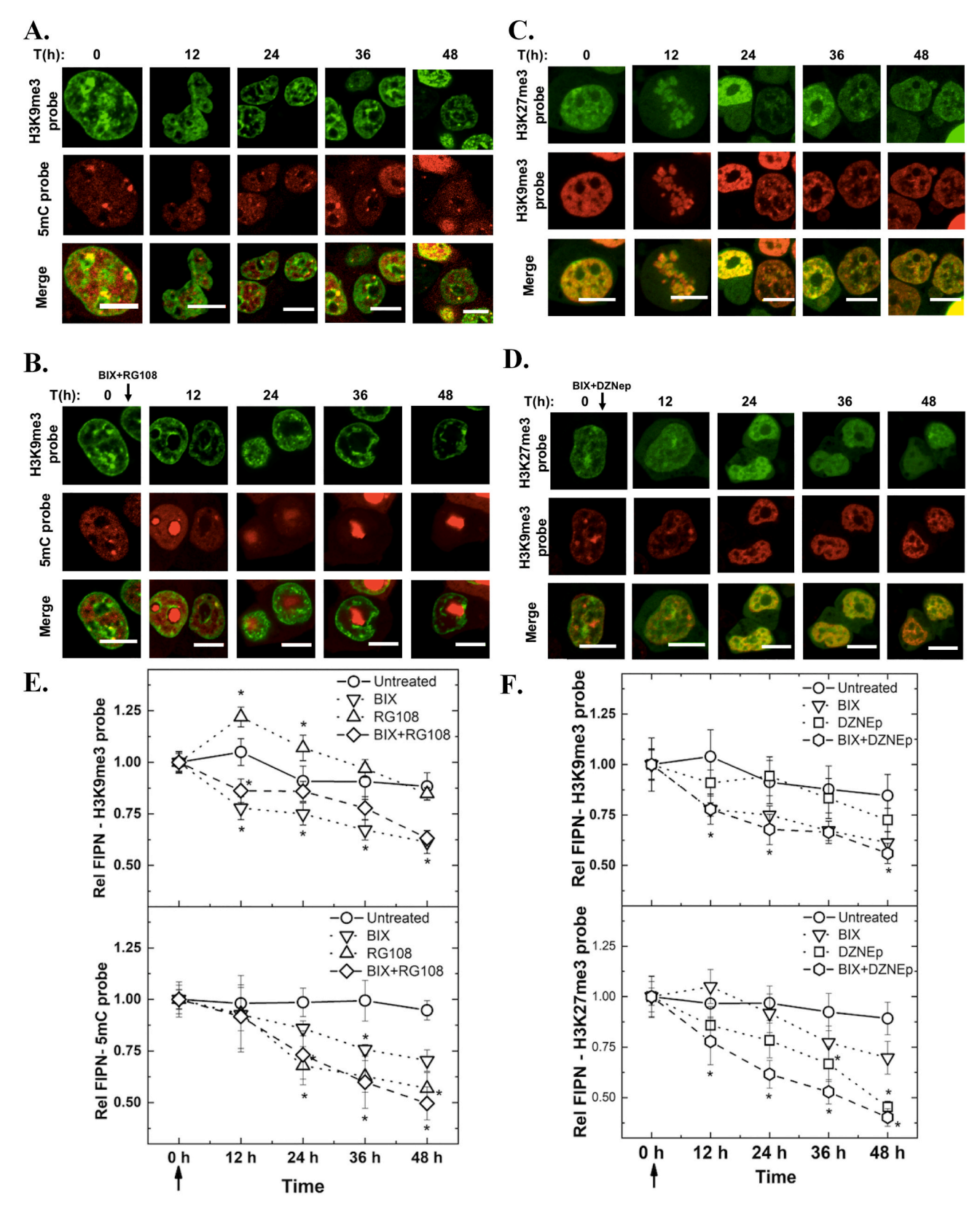


**Fig. 3. A.** HEK293T cells were transfected with the H3K9me3 and 5mC probes and imaged at successive time points. The cells undergo division and the daughter cells express both probes with distinctive patterns of heterochromatin. In **B**, the same probe sets are introduced in cells exposed to RG108 and BIX01294 which lower the histone methylation levels (arrow indicates the time of addition of the drug). The pattern is lost over time as the drug decreases the binding sites available for the probes. In **C** and **D**, the probe combination tested is H3K9me3 and DNA methylation with or without the addition of BIX01294 and DZNep. In E and F, the mean foci intensity at various time points is captured for both cases along with the data for individual drug exposures (shown in dotted lines). The \* indicates statistically significant differences (p < 0.05) from the untreated case, following a One-Way ANOVA, Tukey's post hoc, p = 30 cells.

observed at the pericentromeric heterochromatin, though a similar decrease in H3K9me3 levels is not observed in DNMT knockout cells [66]. It is thus possible that a decrease in H3K9me3 induced by BIX01294 can lead to a decrease in DNA methylation levels as well. Readers of methylation marks, such as MeCP2 are present along with H3K9me3 at cHC and interact with HMT's, but the loss of these readers may not necessarily decrease the H3K9me3 levels [69].

After developing an understanding of how the cHC landscape might be altered with drug perturbations, we examined the fHC which is less organized and spatially distinct from the cHC. Our goal was to distinguish these two areas from each other and monitor their potential overlap as chromatin landscape is perturbed. Since DNA methylation and H3K27me3 are both associated with the fHC, we chose to use the H3K9me3 and H3K27me3 probes together since these modifications are usually spatially distinct [70] with evidence of cross-talk at selective gene loci [71]. We monitored simultaneous changes in cHC and fHC as cells undergo growth and division (see Fig. 3C and D). As the cell pictured at T = 0 h in Fig. 3C at the time undergoes division (at T = 12h), the H3K27me3 modification is associated with the chromosomes and also expressed in the daughter cells. The pattern of binding seen with the H3K27me3 probe in Fig. 3C is retained upon cell division. Similarly, the H3K9me3 probe is associated with the nuclear periphery and shows the characteristic pattern of cHC. The daughter cells retain this pattern upon division. There is little overlap between the probes as is expected with these two modifications [71]. The change in mean foci intensity with time is presented in Fig. 3F where the signal obtained by both probes is steady with some decline at the last time point. cHC and fHC were then perturbed by the addition DZNep and BIX01294 both at final concentrations of 5 µM (see Fig. 3D). Immediately following drug addition (at the 12 h time point), the cumulative effect of the drugs on both modifications is a loss in the signal. This change is more prominent at increasing time points with the signal becoming more diffuse as H3K9me3 and H3K27me3 levels decrease. Data from single drug exposure for each probe (see dashed lines in Fig. 3F and cell images in Fig. S8C and D (Supporting Information)) provide some understanding of the observed effects. The addition of DZNep counters the slight increase in H3K9me3 levels seen in the untreated case (at T = 0 h). The modification level remains steady at increasing exposure time and is similar to the untreated case at T = 48 h. The overall effect of adding BIX01294 and DZNep is a lowering of the H3K9me3 level that is very similar to the effects of adding BIX01294 alone. The addition of BIX01294 interestingly increases the H3K27me3 levels 12 h after exposure, though this trend is not maintained over successive time points. The addition of DZNep causes a sharp decline in the H3K27me3 levels. The cumulative effects of adding two drugs is not entirely an additive effect of individual drugs (at  $T>12~\mathrm{h}$ ), indicating that synergistic mechanisms might be at work. It has been previously reported that the loss of histone methyltransferase specific for H3K9 and subsequent decrease in H3K9me3 can lead to a redistribution of H3K27me3 in mouse cells [57] or a gain of H3K27me3 in fungi [72] which aligns with our observations here. Additional single cell images for both treated and untreated cases along with the phase contrast images of the grid slide coordinates is presented in Fig. S7B and D (Supporting Information).

Finally, dynamic trajectories of single cells can be obtained by following an individual cell as it undergoes division and quantifying the mean foci intensities of the original and divided populations. The data for single cell modulation of epigenetic levels upon combinatorial drug exposure is presented in Fig. S9 (Supporting Information) for five cells with each of the probe sets.

## 3.4. Heterochromatin regions identified by FRET

Techniques available for the detection of histone PTMs and DNA methylation are presently limited to detecting single modifications. Some tool sets relying on multivalent domains or bimolecular fluorescence complementation (BiFC) have been developed for the detection of

bivalent chromatin and epigenetic modifications at repetitive regions of the genome [73]. However, there are some limitations to these tools, namely the signal-to-noise ratio and localization of multivalent sensors [74] and the irreversible signal generated by BiFC probes [75]. An alternate FRET based approach is offered by the probes developed in this study to visualize epigenetic modifications that co-exist on the nucleosome level (schematic presented in Fig. 4A). The mEGFP and mCherry fluorescent moieties form a well-established FRET pair [76–77] and can be used for the simultaneous visualization of two epigenetic modifications.

We first demonstrated the feasibility of using the fluorescent probes as a FRET pair by constructing a FRET positive control plasmid consisting of an mEGFP fluorophore connected by a flexible linker to an mCherry fluorophore, driven by the same CMV promoter present in the probes and containing an NLS signal (see Fig. S10A (Supporting Information) for a schematic). A strong FRET interaction is expected between the pair since the short flexible linker allows for free rotation. A negative control (see Fig. S10B (Supporting Information)) consisting of an mEGFP-only and an mCherry-only plasmid co-transfected together was used. In the latter case, no (or low) FRET is expected since the two fluorophores will be freely diffusing in the nucleus and will not be within the nanometer range (<10 nm) in which FRET interactions are expected. The Positive and Negative FRET control samples were imaged with FRET index and NFRET images determined as shown in Fig. S10B (Supporting Information).

We then introduced a pair of epigenetic probes (one with an EGFP (G) and the other with an mCherry (R) tag). Five combinations of epigenetic probes were tested, namely H3K9me3(G)-5mC(R), H3K27me3(G)-H3K9me3(R), H3K27me3(G)-5mC(R), and H3K9me3 (G)-H3K9me3(R) and H3K9me3(G)-H3K14ac(R). FRET image analysis provides two read-outs, namely FRET-index and NFRET. FRET-index is an absolute FRET value calculated based on donor, acceptor, and FRET images while NFRET is normalized by accounting for the expression level of donor and acceptors at the selected pixel locations. The NFRET value is thus expected to indicate the degree of co-localization at different locations. H3K9me3(G)-H3K9me3(R) pair is used as a positive control, since they were expected to bind to heterochromatin regions in proximity and thus lead to high FRET index and NFRET per cell. The results are summarized in Figs. 4B and S11A and S12A (Supporting Information). H3K14ac probes were developed by our group previously [24] and tags euchromatin regions, while H3K9me3 is expected to tag heterochromatin regions. We then used H3K9me3(G)-H3K14ac(R) as a negative control. FRET images of H3K9me3(G)-H3K14ac(R) are summarized in Fig. S11B (Supporting Information) with no discernable FRET interactions as expected.

We then proceeded to delineate regions in heterochromatin enriched with different combinations of silencing marks using H3K9me3(G)-5mC (R), H3K27me3(G)-H3K9me3(R), and H3K27me3(G)-5mC(R) pairs. Significant FRET signals were detected between the 5mC and H3K9me3 probe as shown in Fig. 4B. Although the signal is weaker than the positive FRET control, there is a significant NFRET value after accounting for expression level normalization. To obtain a quantitative comparison among FRET efficiency in different probe sets, we calculated relative NFRET of each pair normalized to NFRET values of our positive FRET control. The relative NFRET value of the H3K9me3(G)-5mC(R) combination is 70% of the H3K9me3-H3K9me3 pair (see also Fig. 4C) further confirmation the strong co-location of H3K9me3 and 5mC probes. These two modifications are expected to enrich in the cHC. A strong FRET signal indicats that these two probes can be found within less than 10 nm of each other comparable to the diameter of a typical nucleosome core particle. The co-localized features are expected to be representative of cHC and more images of co-transfected cells can be found in Fig. S12B (Supporting Information). High-FRET foci are highlighted at the nuclear periphery and at the heterochromatin at the periphery of the nucleolus. Weaker FRET signals are observed in cells transfected with H3K27me3 (G)-H3K9me3(R) and H3K27me3(G)-5mC(R) probes (see also

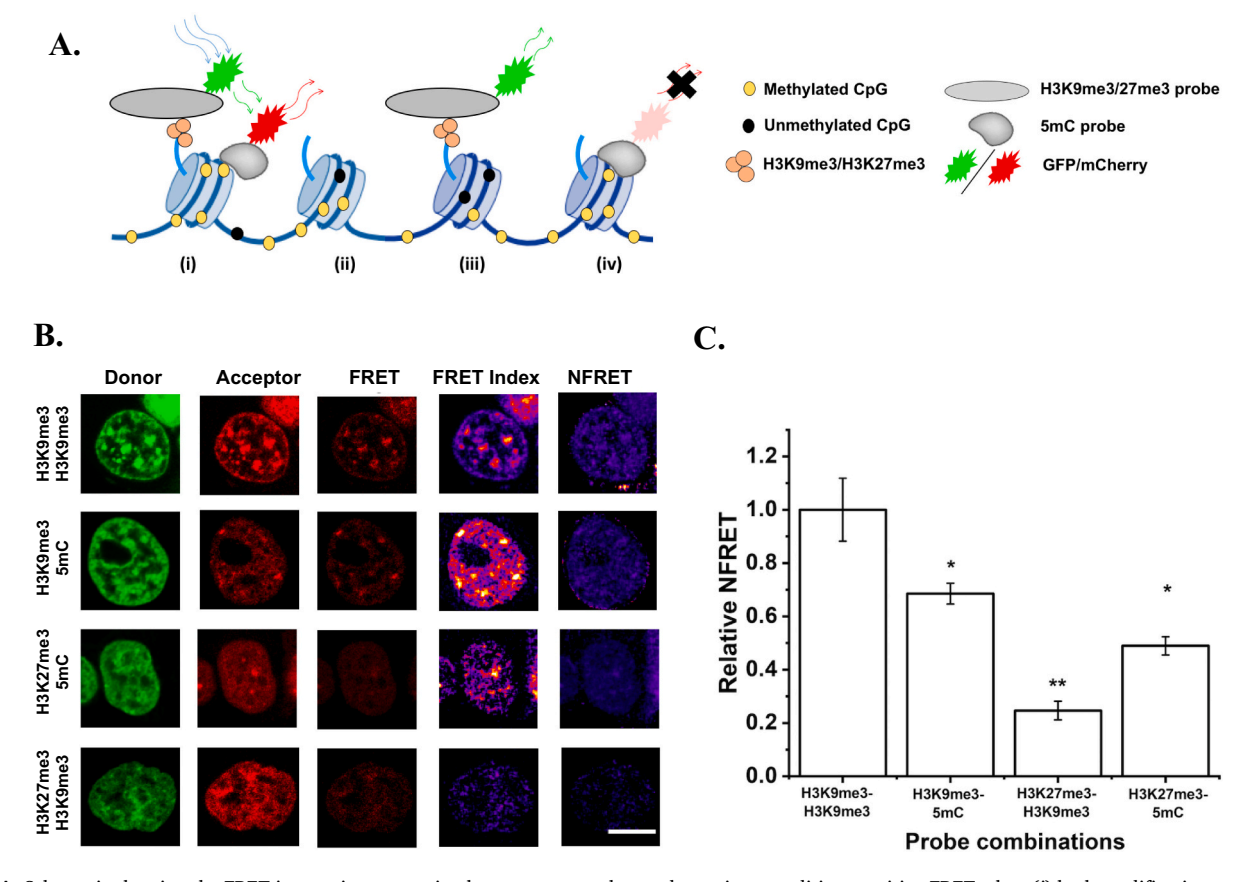


**Fig. 4. A.** Schematic showing the FRET interactions occurring between two probes under various conditions positive FRET when (i) both modifications present and no FRET when (i) no modifications or (iii) and (iv) single modifications are present. **B.** FRET occurring between the various probe sets. The FRET index is an absolute FRET value whereas the NFRET is normalized by taking the donor and acceptor expression levels into account. In **C**, the relative NFRET between different probe sets is quantified. n > 30. \*: p < 0.05, \*\*: p < 0.01.

Fig. S12C and D (Supporting Information)). The relative NFRET values were found to be  $\sim\!25$  and 50% for these two combinations, respectively. 5mC and H3K27me3 are commonly found in fHC, e.g., the inactive X chromosome and autosomally imprinted loci [14]. Bright areas of colocalized modifications of  $<\!100$  nm in size are abundant inside cell nucleus with high FRET index. These areas are notably much smaller than co-localized foci observed using H3K9me3(G)-5mC(R) probes. Among all combinations of the selected epigenetic silencing marks, H3K27me3(G)-H3K9me3(R) probes have the lowest FRET signal (see also Fig. S12D (Supporting Information)). These two probes are mutually exclusive in most nuclear compartments but are known to interact in certain genomic loci, such as telomeres [78], bivalent promoters [78–79] and the inactive X chromosome [80]. Scattered co-localization signals can be detected across nucleus with some co-localized spots near the nuclear periphery.

Overall, we have shown the feasibility of quantifying key epigenetic marks in the cHC and fHC, as well as, tracking changes in these heterochromatin regions via epigenetic "reader" sensors coupled to FRET. Since our sensors are expressed *in situ*, the application of our probes is thus limited to cells that can be successfully transfected. FRET signal can be detected between two probes in a close proximity, i.e., <10 nm (100 Å) [81] and thus is not suitable for co-tracking of two probes far away from each other. Our probes offer live cell tracking capability by identifying specific epigenetic modifications that is otherwise not feasible using conventional cell staining techniques, i.e., hematoxylin staining [82] or cell lysate-based assays, e.g., a sonication based assay [83]. Furthermore, it is important to note that epigenetic regulation of chromatin is an evolving field. It is thus imperative to account for the emerging roles of epigenetic modifications when interpreting the probe

tracking data. Pertinent to our work, H3K9me3 has been recently found to partake in the formation of facultative heterochromatin particularly in stem cells and preadipocytes by recruiting the SETDB1-MBD1-MCAF1 complex [84]. Similarly, H3K9me3 was found to be installed in facultative heterochromatin in an H3K4me3-dependent manner in *Neurospora crassa* [85]. The overall percentage of H3K9me3 found in facultative heterochromatin region, however, remains low at  $\sim\!3.2\%$  [83].

## 4. Conclusions

We developed a sensing platform for simultaneous tracking of multiple epigenetic features inside cell nucleus. Combinations of various epigenetic features, particularly silencing markers, will allow us to monitor and distinguish heterochromatin regions (e.g., constitutive vs. facultative) over time with and without external perturbations. The ability to perform FRET images using two probes enables us to track chromatin region with bivalent features, most likely co-exist within a single nucleosome and monitor their dynamic changes over time.

#### CRediT authorship contribution statement

Conceptualization: AM, OS, JX and CY.
Methodology: AM, OS, JX, LL, AC and CY.
Validation: AM, OS, JX, LL and AC.
Formal Analysis/Investigation: AM, OS, and JX.
Data Curation: AM, OS, and JX.
Writing: AM, OS, and JX.
Visualization: AM, OS, and JX.

Supervision/Project Administration: AM, OS and CY. Funding acquisition: CY.

## Declaration of competing interest

The authors declare that they have no known competing financial interests or personal relationships that could have appeared to influence the work reported in this paper.

#### Acknowledgements

This work was supported by the National Science Foundation [CBET-1512285, CBET-1705560 & EF-1935226]. Support from the Purdue Center for Cancer Research Pilot Grant Program is gratefully acknowledged.

## Appendix A. Supplementary data

Supplementary data to this article can be found online at https://doi.org/10.1016/j.bbagrm.2021.194725.

#### References

- T. Cremer, C. Cremer, Chromosome territories, nuclear architecture and gene regulation in mammalian cells, Nat. Rev. Genet. 2 (4) (2001) 292–301.
- [2] N. Saksouk, E. Simboeck, J. Déjardin, Constitutive heterochromatin formation and transcription in mammals, Epigenetics Chromatin 8 (1) (2015) 1–17.
- [3] J. Wang, S.T. Jia, S. Jia, New insights into the regulation of heterochromatin, Trends Genet. 32 (5) (2016) 284–294.
- [4] B.D. Fodor, N. Shukeir, G. Reuter, T. Jenuwein, Mammalian Su (var) genes in chromatin control, Annu. Rev. Cell Dev. Biol. 26 (2010) 471–501.
- [5] I. Rajapakse, M. Groudine, On emerging nuclear order, J. Cell Biol. 192 (5) (2011) 711–721.
- [6] T. Misteli, Beyond the sequence: cellular organization of genome function, Cell 128 (4) (2007) 787–800.
- [7] J. Dekker, L. Mirny, The 3D genome as moderator of chromosomal communication, Cell 164 (6) (2016) 1110–1121.
- [8] D.U. Gorkin, D. Leung, B. Ren, The 3D genome in transcriptional regulation and pluripotency, Cell Stem Cell 14 (6) (2014) 762–775.
- [9] M. Ruiz-Velasco, J.B. Zaugg, Structure meets function: how chromatin organisation conveys functionality, Curr. Opin. Syst. Biol. 1 (2017) 129–136.
- [10] A.R. Leitch, Higher levels of organization in the interphase nucleus of cycling and differentiated cells, Microbiol. Mol. Biol. Rev. 64 (1) (2000) 138–152.
- [11] F. Santos, B. Hendrich, W. Reik, W. Dean, Dynamic reprogramming of DNA methylation in the early mouse embryo, Dev. Biol. 241 (1) (2002) 172–182.
- [12] C. Guetg, P. Lienemann, V. Sirri, I. Grummt, D. Hernandez-Verdun, M.O. Hottiger, M. Fussenegger, R. Santoro, The NoRC complex mediates the heterochromatin formation and stability of silent rRNA genes and centromeric repeats, EMBO J. 29 (13) (2010) 2135–2146.
- [13] J.A. Lessard, G.R. Crabtree, Chromatin regulatory mechanisms in pluripotency, Annu. Rev. Cell Dev. Biol. 26 (2010) 503–532.
- [14] P. Trojer, D. Reinberg, Facultative heterochromatin: is there a distinctive molecular signature? Mol. Cell 28 (1) (2007) 1–13.
- [15] S. Bartolomé, A. Bermúdez, J.-R. Daban, Internal structure of the 30 nm chromatin fiber, J. Cell Sci. 107 (11) (1994) 2983–2992.
- [16] S.J. Yan, S.J. Lim, S. Shi, P. Dutta, W.X. Li, Unphosphorylated STAT and heterochromatin protect genome stability, FASEB J. 25 (1) (2011) 232–241.
- [17] S.I. Grewal, S. Jia, Heterochromatin revisited, Nat. Rev. Genet. 8 (1) (2007) 35-46.
- [18] J.C. Peng, G.H. Karpen, H3K9 methylation and RNA interference regulate nucleolar organization and repeated DNA stability, Nat. Cell Biol. 9 (1) (2007) 25–35.
- [19] Carone, D. M.; Lawrence, J. B. In Heterochromatin instability in cancer: from the Barr body to satellites and the nuclear periphery, Seminars in cancer biology, Elsevier: 2013; pp 99–108.
- [20] A.H. Fischer, C. Zhao, Q.K. Li, K.S. Gustafson, I.E. Eltoum, R. Tambouret, B. Benstein, L.C. Savaloja, P. Kulesza, The cytologic criteria of malignancy, J. Cell. Biochem. 110 (4) (2010) 795–811.
- [21] C.L. Martin, D. Warburton, Detection of chromosomal aberrations in clinical practice: from karyotype to genome sequence, Annu. Rev. Genomics Hum. Genet. 16 (2015) 309–326.
- [22] R. Srivastava, N. Mishra, Understanding heterochromatin characterization through chromosome banding, J. Biol. Sci. Med. 1 (1) (2015) 11–20.
- [23] B. Hübner, M. Lomiento, F. Mammoli, D. Illner, Y. Markaki, S. Ferrari, M. Cremer, T. Cremer, Remodeling of nuclear landscapes during human myelopoietic cell differentiation maintains co-aligned active and inactive nuclear compartments, Epigenetics Chromatin 8 (1) (2015) 47.
- [24] O.F. Sanchez, A. Mendonca, A.D. Carneiro, C. Yuan, Engineering recombinant protein sensors for quantifying histone acetylation, ACS Sensors 2 (3) (2017) 426–435.

- [25] O.F. Sánchez, A. Mendonca, A. Min, J. Liu, C. Yuan, Monitoring histone methylation (H3K9me3) changes in live cells, ACS Omega 4 (8) (2019) 13250–13259.
- [26] K.I. Albanese, M.W. Krone, C.J. Petell, M.M. Parker, B.D. Strahl, E.M. Brustad, M. L. Waters, Engineered reader proteins for enhanced detection of methylated lysine on histones, ACS Chem. Biol. 15 (1) (2020) 103–111.
- [27] H.F. Jørgensen, K. Adie, P. Chaubert, A.P. Bird, Engineering a high-affinity methyl-CpG-binding protein, Nucleic Acids Res. 34 (13) (2006) e96.
- [28] S.J. Tekel, D.A. Vargas, L. Song, J. LaBaer, M.R. Caplan, K.A. Haynes, Tandem histone-binding domains enhance the activity of a synthetic chromatin effector, ACS Synth. Biol. 7 (3) (2018) 842–852.
- [29] W. Fischle, H. Franz, S.A. Jacobs, C.D. Allis, S. Khorasanizadeh, Specificity of the chromodomain Y chromosome family of chromodomains for lysine-methylated ARK (S/T) motifs, J. Biol. Chem. 283 (28) (2008) 19626–19635.
- [30] J. Min, Y. Zhang, R.-M. Xu, Structural basis for specific binding of polycomb chromodomain to histone H3 methylated at Lys 27, Genes Dev. 17 (15) (2003) 1823–1828.
- [31] S.-E. Kim, M. Chang, C. Yuan, One-pot approach for examining the DNA methylation patterns using an engineered methyl-probe, Biosens. Bioelectron. 58 (2014) 333–337.
- [32] W. Fischle, Y. Wang, S.A. Jacobs, Y. Kim, C.D. Allis, S. Khorasanizadeh, Molecular basis for the discrimination of repressive methyl-lysine marks in histone H3 by polycomb and HP1 chromodomains, Genes Dev. 17 (15) (2003) 1870–1881.
- [33] Dong, C.; Liu, Y.; Lyu, T.-J.; Beldar, S.; Lamb, K. N.; Tempel, W.; Li, Y.; Li, Z.; James, L. I.; Qin, S., Structural basis for the binding selectivity of human CDY chromodomains. Cell Chemical Biology 2020, 27 (7), 827–838. e7.
- [34] Qin, S.; Li, L.; Min, J., The Chromodomain of Polycomb: Methylation Reader and Beyond. In Polycomb Group Proteins, Elsevier: 2017; pp 33–56.
- [35] R.S. Stein, N. Li, W. He, E. Komives, W. Wang, Recognition of methylated peptides by Drosophila melanogaster polycomb chromodomain, J. Proteome Res. 12 (3) (2013) 1467–1477.
- [36] Phelan, K.; May, K. M., Basic techniques in mammalian cell tissue culture. Current protocols in cell biology 2015, 66 (1), 1.1. 1–1.1. 22.
- [37] M. Swarnalatha, A.K. Singh, V. Kumar, The epigenetic control of E-box and Mycdependent chromatin modifications regulate the licensing of lamin B2 origin during cell cycle, Nucleic Acids Res. 40 (18) (2012) 9021–9035.
- [38] K. Sidhu, V. Kumar, C-ETS transcription factors play an essential role in the licensing of human MCM4 origin of replication, Biochim. Biophys. Acta, Gene Regul. Mech. 1849 (11) (2015) 1319–1328.
- [39] P. Rajput, V. Pandey, V. Kumar, Stimulation of ribosomal RNA gene promoter by transcription factor Sp1 involves active DNA demethylation by Gadd45-NER pathway, Biochim. Biophys. Acta, Gene Regul. Mech. 1859 (8) (2016) 953–963.
- [40] M.R.C. Charles, A. Mahesh, S.-Y. Lin, H.-P. Hsieh, A. Dhayalan, M.S. Coumar, Identification of novel quinoline inhibitor for EHMT2/G9a through virtual screening, Biochimie 168 (2020) 220–230.
- [41] J.S. Lee, Y. Kim, I.S. Kim, B. Kim, H.J. Choi, J.M. Lee, H.-J.R. Shin, J.H. Kim, J.-Y. Kim, S.-B. Seo, H. Lee, O. Binda, O. Gozani, G.L. Semenza, M. Kim, K.I. Kim, D. Hwang, S.H. Baek, Negative regulation of hypoxic responses via induced reptin methylation, Mol. Cell 39 (1) (2010) 71–85.
- [42] O. Denisenko, D. Mar, M. Trawczynski, K. Bomsztyk, Chromatin changes trigger laminin genes dysregulation in aging kidneys, Aging (Albany NY) 10 (5) (2018) 1133–1145.
- [43] S. Kubicek, R.J. O'Sullivan, E.M. August, E.R. Hickey, Q. Zhang, M.L. Teodoro, S. Rea, K. Mechtler, J.A. Kowalski, C.A. Homon, Reversal of H3K9me2 by a small-molecule inhibitor for the G9a histone methyltransferase, Mol. Cell 25 (3) (2007) 473-481.
- [44] Y. Chang, X. Zhang, J.R. Horton, A.K. Upadhyay, A. Spannhoff, J. Liu, J.P. Snyder, M.T. Bedford, X. Cheng, Structural basis for G9a-like protein lysine methyltransferase inhibition by BIX-01294, Nat. Struct. Mol. Biol. 16 (3) (2009) 312-317
- [45] B. Brueckner, R.G. Boy, P. Siedlecki, T. Musch, H.C. Kliem, P. Zielenkiewicz, S. Suhai, M. Wiessler, F. Lyko, Epigenetic reactivation of tumor suppressor genes by a novel small-molecule inhibitor of human DNA methyltransferases, Cancer Res. 65 (14) (2005) 6305–6311.
- [46] J. Savickiene, G. Treigyte, A. Jazdauskaite, V.V. Borutinskaite, R. Navakauskiene, DNA methyltransferase inhibitor RG108 and histone deacetylase inhibitors cooperate to enhance NB4 cell differentiation and E-cadherin re-expression by chromatin remodelling, Cell Biol. Int. 36 (11) (2012) 1067–1078.
- [47] S. Asgatay, C. Champion, G. Marloie, T. Drujon, C. Senamaud-Beaufort, A. Ceccaldi, A. Erdmann, A. Rajavelu, P. Schambel, A. Jeltsch, Synthesis and evaluation of analogues of N-phthaloyl-l-tryptophan (RG108) as inhibitors of DNA methyltransferase 1, J. Med. Chem. 57 (2) (2014) 421–434.
- [48] T.B. Miranda, C.C. Cortez, C.B. Yoo, G. Liang, M. Abe, T.K. Kelly, V.E. Marquez, P. A. Jones, DZNep is a global histone methylation inhibitor that reactivates developmental genes not silenced by DNA methylation, Mol. Cancer Ther. 8 (6) (2009) 1579–1588.
- [49] J. Tan, X. Yang, L. Zhuang, X. Jiang, W. Chen, P.L. Lee, R.M. Karuturi, P.B.O. Tan, E.T. Liu, Q. Yu, Pharmacologic disruption of Polycomb-repressive complex 2mediated gene repression selectively induces apoptosis in cancer cells, Genes Dev. 21 (9) (2007) 1050–1063.
- [50] Goldstein, M.; Watkins, S., Immunohistochemistry. Current protocols in molecular biology 2008, 81 (1), 14.6. 1–14.6. 23.
- [51] S.V. Costes, D. Daelemans, E.H. Cho, Z. Dobbin, G. Pavlakis, S. Lockett, Automatic and quantitative measurement of protein-protein colocalization in live cells, Biophys. J. 86 (6) (2004) 3993–4003.

- [52] J.N. Feige, D. Sage, W. Wahli, B. Desvergne, L. Gelman, PixFRET, an ImageJ plugin for FRET calculation that can accommodate variations in spectral bleedthroughs, Microsc. Res. Tech. 68 (1) (2005) 51–58.
- [53] A.E. Carpenter, T.R. Jones, M.R. Lamprecht, C. Clarke, I.H. Kang, O. Friman, D. A. Guertin, J.H. Chang, R.A. Lindquist, J. Moffat, CellProfiler: image analysis software for identifying and quantifying cell phenotypes, Genome Biol. 7 (10) (2006) R100.
- [54] B.D. Towbin, C. González-Aguilera, R. Sack, D. Gaidatzis, V. Kalck, P. Meister, P. Askjaer, S.M. Gasser, Step-wise methylation of histone H3K9 positions heterochromatin at the nuclear periphery, Cell 150 (5) (2012) 934–947.
- [55] K.J. McManus, V.L. Biron, R. Heit, D.A. Underhill, M.J. Hendzel, Dynamic changes in histone H3 lysine 9 methylations identification of a mitosis-specific function for dynamic methylation in chromosome congression and segregation, J. Biol. Chem. 281 (13) (2006) 8888–8897.
- [56] A.H. Peters, S. Kubicek, K. Mechtler, R.J. O'Sullivan, A.A. Derijck, L. Perez-Burgos, A. Kohlmaier, S. Opravil, M. Tachibana, Y. Shinkai, Partitioning and plasticity of repressive histone methylation states in mammalian chromatin, Mol. Cell 12 (6) (2003) 1577–1589.
- [57] A.H. Peters, D. O'Carroll, H. Scherthan, K. Mechtler, S. Sauer, C. Schöfer, K. Weipoltshammer, M. Pagani, M. Lachner, A. Kohlmaier, Loss of the Suv39h histone methyltransferases impairs mammalian heterochromatin and genome stability, Cell 107 (3) (2001) 323–337.
- [58] Y. Hori, T. Norinobu, M. Sato, K. Arita, M. Shirakawa, K. Kikuchi, Development of fluorogenic probes for quick no-wash live-cell imaging of intracellular proteins, J. Am. Chem. Soc. 135 (33) (2013) 12360–12365.
- [59] D. Greiner, T. Bonaldi, R. Eskeland, E. Roemer, A. Imhof, Identification of a specific inhibitor of the histone methyltransferase SU (VAR) 3-9, Nat. Chem. Biol. 1 (3) (2005) 143–145.
- [60] F.L. Cherblanc, K.L. Chapman, R. Brown, M.J. Fuchter, Chaetocin is a nonspecific inhibitor of histone lysine methyltransferases, Nat. Chem. Biol. 9 (3) (2013) 136–137.
- [61] D.J. Arndt-Jovin, T.M. Jovin, Analysis and sorting of living cells according to deoxyribonucleic acid content, J. Histochem. Cytochem. 25 (7) (1977) 585–589.
- [62] E. Heard, C.M. Disteche, Dosage compensation in mammals: fine-tuning the expression of the X chromosome, Genes Dev. 20 (14) (2006) 1848–1867.
- [63] R. Feil, F. Berger, Convergent evolution of genomic imprinting in plants and mammals, Trends Genet. 23 (4) (2007) 192–199.
- [64] E. Viré, C. Brenner, R. Deplus, L. Blanchon, M. Fraga, C. Didelot, L. Morey, A. Van Eynde, D. Bernard, J.-M. Vanderwinden, The Polycomb group protein EZH2 directly controls DNA methylation. Nature 439 (7078) (2006) 871–874.
- [65] T.V. Sekar, K. Foygel, J.G. Gelovani, R. Paulmurugan, Genetically encoded molecular biosensors to image histone methylation in living animals, Anal. Chem. 87 (2) (2015) 892–899.
- [66] B. Lehnertz, Y. Ueda, A.A. Derijck, U. Braunschweig, L. Perez-Burgos, S. Kubicek, T. Chen, E. Li, T. Jenuwein, A.H. Peters, Suv39h-mediated histone H3 lysine 9 methylation directs DNA methylation to major satellite repeats at pericentric heterochromatin, Curr. Biol. 13 (14) (2003) 1192–1200.
- [67] J. Sharif, M. Muto, S.-I. Takebayashi, I. Suetake, A. Iwamatsu, T.A. Endo, J. Shinga, Y. Mizutani-Koseki, T. Toyoda, K. Okamura, The SRA protein Np95 mediates epigenetic inheritance by recruiting Dnmt1 to methylated DNA, Nature 450 (7171) (2007) 908–912.
- [68] S.B. Rothbart, K. Krajewski, N. Nady, W. Tempel, S. Xue, A.I. Badeaux, D. Barsyte-Lovejoy, J.Y. Martinez, M.T. Bedford, S.M. Fuchs, Association of UHRF1 with methylated H3K9 directs the maintenance of DNA methylation, Nat. Struct. Mol. Biol. 19 (11) (2012) 1155.

- [69] Y. Jiang, A. Matevossian, Y. Guo, S. Akbarian, Setdb1-mediated histone H3K9 hypermethylation in neurons worsens the neurological phenotype of Mecp2deficient mice, Neuropharmacology 60 (7–8) (2011) 1088–1097.
- [70] J. Kim, H. Kim, Recruitment and biological consequences of histone modification of H3K27me3 and H3K9me3, ILAR J. 53 (3–4) (2012) 232–239.
- [71] J. Boros, N. Arnoult, V. Stroobant, J.-F. Collet, A. Decottignies, Polycomb repressive complex 2 and H3K27me3 cooperate with H3K9 methylation to maintain heterochromatin protein 1α at chromatin, Mol. Cell. Biol. 34 (19) (2014) 3662–3674.
- [72] K. Jamieson, E.T. Wiles, K.J. McNaught, S. Sidoli, N. Leggett, Y. Shao, B.A. Garcia, E.U. Selker, Loss of HP1 causes depletion of H3K27me3 from facultative heterochromatin and gain of H3K27me2 at constitutive heterochromatin, Genome Res. 26 (1) (2016) 97–107.
- [73] C. Lungu, S. Pinter, J. Broche, P. Rathert, A. Jeltsch, Modular fluorescence complementation sensors for live cell detection of epigenetic signals at endogenous genomic sites, Nat. Commun. 8 (1) (2017) 1–13.
- [74] Delachat, A. M.-F.; Guidotti, N.; Bachmann, A. L.; Meireles-Filho, A. C.; Pick, H.; Lechner, C. C.; Deluz, C.; Deplancke, B.; Suter, D. M.; Fierz, B., Engineered multivalent sensors to detect coexisting histone modifications in living stem cells. Cell chemical biology 2018, 25 (1), 51–56. e6.
- [75] Y. Kodama, C.-D. Hu, Bimolecular fluorescence complementation (BiFC): a 5-year update and future perspectives, Biotechniques 53 (5) (2012) 285–298.
- [76] B.T. Bajar, E.S. Wang, S. Zhang, M.Z. Lin, J. Chu, A guide to fluorescent protein FRET pairs, Sensors 16 (9) (2016) 1488.
- [77] L. Albertazzi, D. Arosio, L. Marchetti, F. Ricci, F. Beltram, Quantitative FRET analysis with the EOGFP-mCherry fluorescent protein pair, Photochem. Photobiol. 85 (1) (2009) 287–297.
- [78] S. Bilodeau, M.H. Kagey, G.M. Frampton, P.B. Rahl, R.A. Young, SetDB1 contributes to repression of genes encoding developmental regulators and maintenance of ES cell state, Genes Dev. 23 (21) (2009) 2484–2489.
- [79] R.D. Hawkins, G.C. Hon, L.K. Lee, Q. Ngo, R. Lister, M. Pelizzola, L.E. Edsall, S. Kuan, Y. Luu, S. Klugman, Distinct epigenomic landscapes of pluripotent and lineage-committed human cells, Cell Stem Cell 6 (5) (2010) 479–491.
- [80] M. Escamilla-Del-Arenal, S. Da Rocha, C. Spruijt, O. Masui, O. Renaud, A.H. Smits, R. Margueron, M. Vermeulen, E. Heard, Cdyl, a new partner of the inactive X chromosome and potential reader of H3K27me3 and H3K9me2, Mol. Cell. Biol. 33 (24) (2013) 5005–5020.
- [81] R.B. Sekar, A. Periasamy, Fluorescence resonance energy transfer (FRET) microscopy imaging of live cell protein localizations, J. Cell Biol. 160 (5) (2003) 629–633.
- [82] F. Kimura, T. Kobayashi, R. Kanai, Y. Kobayashi, O. Yuhi, H. Ota, M. Yamaguchi, Y. Yokokawa, T. Uehara, K. Ishii, Image quantification technology of the heterochromatin and euchromatin region for differential diagnosis in the lobular endocervical glandular hyperplasia, Diagn. Cytopathol. 47 (6) (2019) 553–563.
- [83] Becker, J. S.; McCarthy, R. L.; Sidoli, S.; Donahue, G.; Kaeding, K. E.; He, Z.; Lin, S.; Garcia, B. A.; Zaret, K. S., Genomic and Proteomic Resolution of Heterochromatin and Its Restriction of Alternate Fate Genes. Molecular Cell 2017, 68 (6), 1023–1037 e15
- [84] Y. Matsumura, R. Nakaki, T. Inagaki, A. Yoshida, Y. Kano, H. Kimura, T. Tanaka, S. Tsutsumi, M. Nakao, T. Doi, K. Fukami, Timothy F. Osborne, T. Kodama, H. Aburatani, J. Sakai, H3K4/H3K9me3 bivalent chromatin domains targeted by lineage-specific DNA methylation pauses adipocyte differentiation, Mol. Cell 60 (4) (2015) 584–596.
- [85] Q. Zhu, M. Ramakrishnan, J. Park, W.J. Belden, Histone H3 lysine 4 methyltransferase is required for facultative heterochromatin at specific loci, BMC Genomics 20 (1) (2019) 350.